High-frequency neuronal signal better explains multi-phase BOLD response

Qingqing Zhang[a,c,d], **Samuel R. Cramer**[b,c,d], **Kevin L. Turner**[a,c,d], **Thomas Neuberger**[a,c], **Patrick J. Drew**[a,b,c,d,e], **Nanyin Zhang**[a,b,c,d,*]

[a]Department of Biomedical Engineering, The Pennsylvania State University, University Park, USA

[b]The Neuroscience Graduate Program, The Huck Institutes of the Life Sciences, The Pennsylvania State University, University Park, USA

[c]Center for Neurotechnology in Mental Health Research, The Pennsylvania State University, University Park 16802, USA

[d]Center for Neural Engineering, The Pennsylvania State University, University Park 16802, USA

[e]Departments of Engineering Science and Mechanics, Neurosurgery, and Biology, The Pennsylvania State University, University Park, USA

Abstract

Visual stimulation-evoked blood-oxygen-level dependent (BOLD) responses can exhibit more complex temporal dynamics than a simple monophasic response. For instance, BOLD responses sometimes include a phase of positive response followed by a phase of post-stimulus undershoot. Whether the BOLD response during these phases reflects the underlying neuronal signal fluctuations or is contributed by non-neuronal physiological factors remains elusive. When presenting blocks of sustained (i.e. DC) light ON-OFF stimulations to unanesthetized rats, we observed that the response following a decrease in illumination (i.e. OFF stimulation-evoked BOLD response) in the visual cortices displayed reproducible multiple phases, including an initial positive BOLD response, followed by an undershoot and then an overshoot before the next ON trial. This multi-phase BOLD response did not result from the entrainment of the periodic stimulation structure. When we measured the neural correlates of these responses, we found that the high-frequency band from the LFP power (300 – 3000 Hz, multi-unit activity (MUA)), but not the power in the gamma band (30 – 100 Hz) exhibited the same multiphasic dynamics as the

BOLD signal. This study suggests that the post-stimulus phases of the BOLD response can be better explained by the high-frequency neuronal signal.

1. Introduction

Functional magnetic resonance imaging (fMRI) has been widely used to study brain functions with the assumption that it provides an indirect measure of neuronal-related events (Kwong et al., 1992; Ogawa et al., 1992; Pauling and Coryell, 1936). The blood-oxygen-level dependent (BOLD) signal is routinely modeled as a linear convolution of the underlying neuronal signal (e.g., local field potentials (LFPs) or multi-unit activity (MUA)) with a hemodynamic response function (HRF). Indeed, correlated BOLD and neuronal responses have been generally found during sensory stimulation in primary sensory cortex (Angenstein et al., 2009; Drew et al., 2020; Goense and Logothetis, 2008; Kayser, 2004; Lima et al., 2014; Logothetis et al., 2001; Nir et al., 2007; Winder et al., 2017), particularly when the stimulation-evoked BOLD response only displays a positive phase. However, when the BOLD response displays more complex patterns, sometimes including a phase of positive response followed by a phase of post-stimulus undershoot, how different BOLD phases, especially the post-stimulus undershoot, relate to neuronal activities remain unclear (Shmuel et al., 2006; Winder et al., 2017).

Previous work suggests that BOLD undershoot could result from the mismatch of the temporal dynamics of individual hemodynamic and metabolic events including changes in cerebral blood flow (CBF), cerebral blood volume (CBV), cerebral metabolic rate of oxygen ($CMRO_2$) (Buxton et al., 1998; Lu et al., 2004). However, other work indicates that BOLD undershoot might reflect the post-stimulus reduction of neuronal activity (Shmuel et al., 2006) or the activity of vasoconstrictive neurons (Uhlirova et al., 2016). Understanding the mechanism underlying different BOLD phases is of critical importance for the interpretation of BOLD data, particularly in relation to variable behavioral responses during different BOLD phases.

In our recent study (Zhang et al., 2022), we found that sustained (i.e. DC) light ON-OFF stimulations can induce a reproducible multi-phase BOLD response in the visual cortices, with a clear BOLD undershoot during the OFF response. Interestingly, this BOLD undershoot can gradually return to positive activation before the light onset of the next trial. To elucidate the neuronal basis of this BOLD response pattern, here we conducted electrophysiological recording in a separate group of animals using the identical visual stimulation paradigm. We found that the multi-phase BOLD response reflected one neuronal responsive feature to the visual stimulation. Instead of being highly correlated with the gamma-range LFP power during sensory stimulations, the BOLD signal fluctuated in the same way as the MUA power (300 – 3000 Hz). The higher frequency range LFP (150 – 250 Hz) shared more similarities with the MUA than gamma-range LFP. Therefore, the post-stimulus phases of the BOLD response might be better explained by the power in the MUA band (i.e. the high-frequency neuronal signal).

2. Results

We separately performed fMRI and electrophysiology experiments during sustained (i.e. DC) light ON-OFF stimulations to unilateral eyes in unanesthetized rats (Fig. 1A, left). During both experiments rats were restrained with a 3D-printed restrainer. The fMRI data were collected in two separate groups of animals, each with a different radiofrequency (RF) coil (referred to as the 3- and 4- channel coils, respectively). In both fMRI and electrophysiology experiments, two visual stimulation paradigms were used, fixed and randomized stimulations. For the fixed stimulation, the ON/OFF duration per trial was 25 s. For the randomized stimulation, the ON/OFF duration per trial was drawn from a uniform distribution of 10 – 30 s (Fig. 1A, right). Each run (15 min) started with a 5-min resting-state recording (i.e. without visual stimulation), followed by the ON-OFF visual stimulation paradigm (10 min). Data acquired during the resting state were defined as the baseline for the run, and all ON and OFF trials were normalized to the same baseline in the run. This analysis was the same for both fMRI and electrophysiology data.

2.1. Post-stimulus BOLD undershoot and pre-ON BOLD overshoot in the right visual areas

We first analyzed the BOLD responses to sustained ON-OFF visual stimulations delivered to the left eye of unanesthetized rats (Zhang et al., 2022). To visualize the temporal evolution of the BOLD signal, we first time-lock averaged fMRI frames across trials for the fixed stimulation paradigm. Figs. S1&S2 show the videos of the averaged spatiotemporal BOLD patterns of the ON and OFF responses from the 3-channel and 4-channel coil, respectively. Surprisingly, we observed that voxels within the right visual areas (rV1/V2, referred to as rVA hereinafter) showed positive response even before the onset of the ON stimulation (referred to as pre-ON activation hereinafter). This pattern was consistent in the two datasets separately collected with two RF coils (Fig. 1C), indicating that this BOLD temporal pattern is reproducible across animals and experimental setup. Compared to the ON-stimulation evoked response (Fig. 1C at 1 s, and also shown in Fig. 1 in (Zhang et al., 2022)), this pre-ON activation spatially covered smaller visual areas, but predominantly existed in the stimulation responsive hemisphere (i.e., the right hemisphere).

To test whether this pre-ON activation was in any way related to the immediate following ON stimulation (e.g. anticipation of the trial onset shown in (Cardoso et al., 2019; Sirotin and Das, 2009)), in each recording session (15 mins, ~11 ON-OFF cycles) we randomly omitted ON stimulations in 2 – 3 trials. We then time-lock averaged the fMRI frames across those omitted-ON trials. Voxels within the rVA persistently showed positive activation around the potential light onset that was omitted (Fig. 1E, one sample t-test, one tail, $p = 5 \times 10^{-14}$). To further quantify the pre-ON BOLD response features, voxels displaying significant positive BOLD responses around the potential light onset in the rVA were selected (defined as rVA*, see Methods). The cross-trial averaged time courses of the rVA* suggested that this pre-ON activation started from the late OFF period of the immediate preceding OFF trials and was sustained until the end of the whole omitted-ON trials (Fig. 1D). This long-lasting positive response indicates the anticipatory effect in the BOLD response (Cardoso et al., 2019; Sirotin and Das, 2009), if existed, was not precise here.

We applied the rVA* masks as used in Fig. 1D to the data collected with the 3- and 4-channel coils during fixed stimulations (Fig. 1F). The ON and OFF time courses had two striking features: (a) an undershoot following the evoked response to the light stimulation onset/offset; and b) in the late OFF period, the response returned to positive and was continuously being positive prior to the next ON stimulation (Fig. 1F). The first feature can also be appreciated from the whole-brain frames: during the undershoot period (8 – 12 s), negative response was localized in the visual areas for the ON trials, and in both the visual areas and superior colliculus for the OFF trials (Figs. 1F, S1–S3, one sample t-test, one tail, ON trials: $p = 3 \times 10^{-9}$, OFF trials: $p = 6 \times 10^{-5}$). These multi-phase BOLD responsive features indicate that a stimulus-relevant mechanism which is specific to this ON-OFF stimulation may contribute to this BOLD response pattern. It also suggests that the pre-ON activation mentioned above might represent a continuous recovery of BOLD response in the late OFF period, instead of an anticipation of the next trial onset shown in (Cardoso et al., 2019; Sirotin and Das, 2009).

2.2. Multi-phase BOLD response in the rVA was not entrained by the periodic stimulation structure

To test whether the multi-phase BOLD response feature (i.e., from post-stimulus undershoot to pre-ON activation) resulted from the entrainment of the periodic structure of ON-OFF stimulations, we analyzed the data in which animals experienced randomized ON-OFF stimulations (Fig. 1A). The BOLD response was time-lock averaged based on the stimulus-ON time across trials. Fig. 1F, derived from the fixed stimulation, suggests that the BOLD signal on average slowly recovered to positive around 20 s post light offset. Therefore, we only averaged the ON trials with the OFF durations in the immediate preceding OFF trials longer than 24 s. The same multi-phase BOLD response pattern, including the post-stimulus undershoot and pre-ON activation, consistently appeared in the rVA* (Fig. 2, one sample t-test, one tail, negative: $p = 0.0017$, positive: $p = 0.0032$), arguing against that this BOLD pattern results from an entraining effect of the periodic structure of visual stimulations. Consistent BOLD response pattern in randomized ON-OFF stimulations again suggests that the pre-ON BOLD activation is not due to the anticipation of the next ON trial, but represents a continuous rebound of BOLD activity in the late OFF period.

2.3. MUA signal shared the same responsive features as the BOLD signal

If the multi-phase response was a neuronal responsive feature to ON-OFF stimulations manifested on the BOLD signal, the underlying neuronal signal would agree with the BOLD signal during ON-OFF stimulations. To test this concept, in a different set of rats ($n = 5$), we recorded neuronal responses of the monocular area of the primary visual cortex (mV1) to the same stimulation paradigms as used in the fMRI experiment outside of the MRI scanner. The low-frequency LFP signal (< 100 Hz) was modulated by stimulations robustly across recordings, but did not show the two characteristic features as the BOLD signal, namely the post-stimulus undershoot and pre-ON activation (Fig. 3B). Visual inspection of the low-frequency LFP spectrogram showed several clustered structures in the graph (Fig. 3A). Based on these clusters, instead of filtering the LFP signal into traditionally defined frequency bands, we separated the signal into 6 bands: 1 – 5 Hz (delta range), 5 – 11 Hz (theta range), 12 – 25 Hz (alpha to beta range), 28 – 50 Hz (low gamma range), 70 – 100

Hz (gamma range), and 150 – 250 Hz, so each clustered feature in the spectrogram remained in one band. The averaged power of each band is shown in Fig. 3B. The 28 – 50 Hz gamma power had a different temporal evolution as the BOLD signal, especially in the OFF period (Fig. 3B). Only power in the higher frequency range LFP (150 – 250 Hz) shared some similarities with the BOLD signal (Fig. 3B).

Since the higher frequency range LFP (150 – 250 Hz) was more correlated with spiking activity (Ray and Maunsell, 2011), we next examined the temporal dynamics of the MUA (300 – 3000 Hz) power. The pattern of the MUA power averaged across trials during the fixed stimulation highly resembled the evolution of the averaged BOLD signal shown in Fig. 1F: (a) an undershoot following the evoked response to the light stimulation onset/offset; b) in the late OFF period, the MUA power went back to positive and was continuously being positive prior to the next ON stimulation (Fig. 4A, S6A, one sample t-test, one tail, ON trials: $p = 9 \times 10^{-4}$, OFF trials: $p = 6 \times 10^{-17}$). Correspondingly, the MUA power remained positive during the omitted-ON trial (Fig. 4B), representing a continuous recovery of neuronal activity in the late OFF period of preceding OFF trials, a feature also presented in the BOLD signal (Fig. 1D).

To test if different baseline normalization methods biased the MUA power time course, instead of using the resting-state (without visual stimulation) signal in the same run as the baseline, we used the signal 2 s before stimulation transition as the baseline for each trial. The MUA power maintained the same responsive features (Fig. S4A). We also Z-score normalized the MUA power, which did not change the responsive features either (Fig. S4B). The MUA power during randomized stimulation remained positive in the late OFF period as well (Figs. S5, S6B, one sample t-test, one tail, $p = 0.0024$).

To better appreciate the temporal similarities between BOLD and MUA power, the averaged OFF time courses of the BOLD signal and MUA (300 – 3000 Hz) power during fixed and randomized stimulations were plotted together (Fig. S7). For both of those two signal modalities (MUA and BOLD), light offset induced an undershoot following the peak response and rebounded to positive before light onset of the next trial. The shared responsive patterns between the BOLD and MUA power suggest a stimulus-relevant neuronal mechanism contributes to the observed multi-phase BOLD activation pattern. Taken together, our study shows that the initial postive BOLD response can be reflected by LFP power in all frequency bands, but the following BOLD phases of undershoot and rebound are better explained by high-frequency neuronal signal.

3. Discussion

The hemodynamic activation preceding the trial onset was previously reported as an anticipatory hemodynamic response in the monkey V1 (Cardoso et al., 2019; Sirotin and Das, 2009), and in the human visual cortex (Burlingham et al., 2022; Griffis et al., 2015; Roth et al., 2020). However, the pre-ON activation observed in our study should not be interpreted as an anticipatory BOLD response but a rebound following the post-stimulus BOLD undershoot, as our finding is different from the previous monkey studies (Cardoso et al., 2019; Sirotin and Das, 2009) at both the behavioral and neuronal levels. Behaviorally,

the rats only passively viewed the visual stimuli, but the monkeys actively performed eye fixation task for a reward. The anticipatory hemodynamic response in the monkey V1 was independent of visual inputs but was entrained by the periodic task structure. Simultaneously recorded neuronal signals (both MUA and LFPs) failed to predict that anticipatory hemodynamic response with the conventional "linear kernel" (i.e., hemodynamic transfer function) convolution approach. In contrast to those findings, the independently recorded BOLD and MUA (300 – 3000 Hz) signals in the present study showed that the responsive patterns across these two modalities were highly consistent. Compared to the gamma range LFP (28 – 50 Hz and 70 – 100 Hz) power, the higher frequency LFP (150 – 250 Hz) power bore higher resemblance with the BOLD signal, maybe due to the "spike bleeding through" the higher frequency LFP range (Ray and Maunsell, 2011). It is important to keep in mind that the activity of neuronal nitric oxide synthathase expressing neurons is not detectable in the LFP, and the activity of these neurons plays an important role in driving sensory evoked dilations and controlling baseline arterial tone (Echagarruga et al., 2020).

The undershoot following stimulation transitions suggests that both neuronal and BOLD signals have a refractory period which constrains responses to fast transitions (a form of visual adaptation). Adaptation is important for information coding in a dynamic environment (Weber and Fairhall, 2019). Using fMRI to study visual adaptation raises many concerns (Larsson et al., 2016). We propose that the BOLD undershoot following the stimulation-related positive response represented a decreased populational neuronal firing. The consistency between the two signals to visual stimulations provides evidence that fMRI can be used to measure adaptation effects over visual hierarchy or be complementary to direct neuronal recordings. This notion is in line with the previous report of dynamic BOLD visual responses that are dependent on stimulation frequencies in awake and anesthetized rodents (Bailey et al., 2013; Dinh et al., 2021; Van Camp et al., 2006)

Previous work studied the neuronal correlates of hemodynamic responses with simultaneous neuronal and hemodynamic signal recordings. Generally, without sensory stimulation, the correlation between neuronal signals and hemodynamic response in the resting state is weak (Winder et al., 2017). During brief sensory stimulations, MUA and LFP have comparable correlations with the hemodynamic signal (Lima et al., 2014; Nunez-Elizalde et al., 2022; Winder et al., 2017). With continuous visual stimulations, in monkey V1, the BOLD signal is more correlated with LFP (20 – 60 Hz) than MUA, in both anesthesia and alert conditions (Goense and Logothetis, 2008; Logothetis et al., 2001). As the temporal frequency of visual stimuli increases, tissue oxygen changes remains correlated with LFP (25 – 90 Hz) but not MUA (Viswanathan and Freeman, 2007). However, in the current study, a qualitative comparison of the neuronal and BOLD signals using the same stimulation paradigms showed that the MUA signal was more correlated with the observed BOLD signal. This suggests that when the evoked BOLD signal exhibits multi-phase response, and when the MUA is not completely coupled with the gamma-range LFP, the MUA power can be a better predictor for the BOLD signal. Neuronal recordings in the monkey V1 showed that the MUA can be as sustained as the LFP signal (Burns et al., 2010) which indicates MUA may contribute to sustained BOLD response as well. However, the non-simultaneous collection of the neuronal and BOLD signals precludes the current study from further analyzing how much variance in the BOLD signal can be explained by the MUA power. Qualitatively, we

noticed that the undershoot in OFF trials was stronger than the undershoot in ON trials in the MUA signal, whereas the BOLD undershoot in OFF trials was not stronger than that in ON trials. One possible reason for this discrepancy is that BOLD undershoot in ON and OFF trials could be underlaid by different types of neuronal activity and/or different neurovascular relationships.

The observed pre-ON BOLD activation draws attention to task designing and modeling the BOLD signal triggered by task events. A prolonged activation/deactivation followed by stimulation may interfere with the response to the following inputs. Previous studies, using awake mice and brief vibrissae stimulation, have found that the HRFs in somatosensory cortex do not show a negative phase, though an undershoot in blood volume was caused by a post-stimulus decrease in neural activity (Winder et al., 2017). When modeling the BOLD response as a linear kernel convolved with the task events (rather than the neuronal signal), the estimated kernel could deviate from the real HRFs. However, it has to be noted that our results should not be interpreted as there is definitely no undershoot in the HRF. In our previous publication (Zhang et al., 2022), we showed that the BOLD undershoot contains both a global component which is contributed by brain-wide ongoing activity and a local component which is from local neuronal responses. It is likely that an undershoot still exists in the HRF. More quantitative assessment of how much of the variance in the BOLD undershoot is attributed to local and global components also requires simultaneous BOLD and electrophysiological recordings in future experiments.

The main significance of this study is that it provides evidence that high-frequency neuronal power resembles the temporal evolution of the BOLD signal when the responsive patterns are complex. The mechanisms governing the undershoot after stimulation onset/offset and the rebound in the late OFF period require further investigations. A whole-field visual stimulation to one eye was used here. The ON/OFF surround inhibition can reduce populational neuronal responses which may contribute to the reduced MUA power after the peak response. Other factors that can modulate stimulation evoked responses include arousal (Niell and Stryker, 2010; Schröder et al., 2020) and body motion (Drew et al., 2019; Musall et al., 2019; Stringer et al., 2019; Winder et al., 2017). In the current study, a strong increase in the power in the 28 – 50 Hz band was seen for the whole OFF period. The frequency range is close to that observed in monkey V1 during visual stimulations (Burns et al., 2010; Ray and Maunsell, 2011). Narrow-band gamma oscillations occurred in a higher frequency range (~60 Hz) in mice (Lee et al., 2014; Niell and Stryker, 2010; Saleem et al., 2017), and may originate from feedforward thalamic input (Saleem et al., 2017). However, the narrow-band gamma oscillation disappeared when mice were in complete darkness (equivalent to the OFF period in the current study) (Saleem et al., 2017). Different neuronal circuits may govern those narrowband oscillations in different stimulation conditions. Whether and how arousal/movement drives the long-lasting narrowband oscillations, and modulates the MUA power in a specific way that is dissociated from the modulation to other frequency bands require further studies.

4. Methods

The fMRI data were collected in a previous study (Zhang et al., 2022). 11 rats were included in the 3-channel dataset and 13 rats were included in the 4-channel dataset. The electrophysiological data was recorded in the current study and 5 rats were included. All experimental procedures were approved by the Pennsylvania State University Institutional Animal Care and Use Committee (IACUC).

4.1. A few definitions

ON trial: response from light onset until light offset.

OFF trial: response from light offset until light onset of the next trial.

Omitted-ON trials: No light ON stimulation following an OFF trial during the fixed ON-OFF stimulation.

4.2. fMRI data collection and preprocessing

The fMRI data were collected on a 7T MRI system interfaced with a Bruker console (Billerica, MA) at the High Field MRI Facility at the Pennsylvania State University. Gradient-echo images were acquired using echo-planar imaging with the parameters: repetition time (TR) = 1 s; echo time (TE) = 15 ms; matrix size = 64×64; FOV = 3.2 $\times$ 3.2 cm^2; slice number = 20; and slice thickness = 1 mm. A TTL signal was sent out from the scanner right after each brain volume collection to ensure the synchronization of visual stimulation and fMRI measurement. Each animal experienced 3 scanning sessions in each recording. Each session was 15 min, with the first 5 min being resting-state scanning and the following 10 min being fixed (ON/OFF duration: 25 s) or randomized (ON/OFF duration: 10 – 30 s) visual stimulations. In the fixed stimulation paradigm, we randomly skipped 2 – 3 ON trials per recording session.

The fMRI signal was preprocessed as: motion scrubbing (the framewise displacement (FD) was calculated, and frames with FD > 0.25 mm and neighboring frames were removed from the corresponding sessions), registration (MIVA, http://ccni.wpi.edu/), motion correction (SPM12, http://www.fil.ion.ucl.ac.uk/spm/), spatial smoothing (FWHM = 0.75 mm), motion regression and detrending. The signal from the first 5 min (resting-state period) was used as the baseline. The signal of each voxel at each time point was Z-scored by subtracting the mean and then dividing the standard deviation of baseline signal for that voxel. The number of trials for fMRI data was summarized in Table 1.

4.3. Definition of brain mask of rVA*

For omitted-ON trials (within each animal), we averaged the whole-brain fMRI response from −3 to 3 s aligned to the potential light onset that was omitted. We then used the 90th percentile of this averaged whole-brain response as the threshold for brain voxels that responded to the potential light onset. The selected voxels were further masked with the functional right visual area (rVA) mask (Zhang et al., 2022) to get the responsive voxels within the rVA, defined as rVA*.

4.4. Electrophysiology surgery

Adult male rats (Long Evans, Charles River, Wilmington, MA, 350 – 400 g) were initially anesthetized by ketamine (40 mg/kg) and xylazine (12 mg/kg). Oxygen without or with isoflurane (0.5 – 1.5%) was ventilated through a nose cone during the whole surgery. Heart rate, body temperature, and SpO2 were monitored (MouseSTAT Jr., Kent Scientific Corporation). A warming pad (PhysioSuite, Kent Scientific Corporation) was used to keep the body temperature at 35 – 37 °C. Three different kinds of electrodes were used in this study: homemade 4-channel tungsten electrode (0.1 – 0.2 MΩ), 4-channel Q-trode (~0.4 MΩ, NeuroNexus, Ann Arbor, MI), and 16-channel chronic electrode (~0.4 MΩ, NeuroNexus, Ann Arbor, MI). The electrode was lowered to the right mV1 (−6.6 to bregma, +3.2 to midline). The uppermost recording site of each electrode was positioned right below the pial surface (~100 μm).

4.5. Electrophysiological recording

The neuronal signal was recorded through the Tucker-Davis Technologies (TDT, Alachua, FL) system with a sampling rate of 24.414 kHz. The raw signal was recorded in the differential mode, so each channel was referenced to its nearby channel to avoid the volume conduction issue (Buzsaki et al., 2012; Kajikawa and Schroeder, 2011; Parabucki and Lampl, 2017).

4.6. Visual stimulation

For the electrophysiological data, we used either a blue laser (473TB-300FC, Shanghai Laser & Optics Century Co., Ltd. as used in the fMRI experiment) or a broadband 460 – 860 nm LED (Thorlabs, Newton, NJ) as the light source for visual stimulations. The light coming out of a patchcord (Doric lenses, Quebec, Canada) was calibrated to 25 – 50 μW. The patchcord tip was placed about 2 cm to the animal's left eye. A TTL pulse from a function generator was used to control the ON and OFF of the light source, which was recorded by the TDT recording system at the same sampling rate as the electrophysiological data (24.414 kHz) recording for synchronization.

During electrophysiology experiments, animals experienced ON-OFF stimulations in the same way as the fMRI experiments (Zhang et al., 2022). Visual stimulations (either fixed or randomized) were presented in 15-min blocks with the first 5 min being resting-state (i.e., no stimulation) recording. For fixed stimulation, the ON/OFF duration was always 25 s, and in each block, we randomly omitted 2 – 3 ON trials. For randomized stimulations, the ON/OFF duration per trial was drawn from a uniform distribution of 10 – 30 s. Randomized stimulations were presented to animals that had never been exposed to fixed visual stimulation before. Animals experienced 3 blocks of fixed stimulations or 3 blocks of randomized stimulations during each recording session.

4.7. Electrophysiological signal preprocessing

For the animals implanted with 4-channel electrodes, with differential recording, each animal provided signals from 2 channels. Because responses from those two channels were highly correlated (the distance between two channels was ∼ 200 μm), we included data of one channel from each animal for the group-level analysis to reduce redundancy. For

animals implanted with 16-channel electrodes, which provided signals from 8 channels, we included data from 4 channels (closer to the brain surface) for the group-level analysis.

4.8. MUA power calculation

The raw signal was filtered to 300 – 3000 Hz with a third-order Butterworth filter (MATLAB functions: butter, zp2sos, filtfilt). The MUA power was calculated by squaring the signal and low pass filtering the result to < 2 Hz (MATLAB functions: butter, zp2sos, filtfilt) to smooth the power trace (Turner et al., 2020). The result was resampled to 30 Hz.

4.9. LFP spectrogram generation

Time-frequency spectrograms were calculated with the Chronux toolbox (function: mtspecgramc, tapers = [5, 9], fpass = [1, 300], movingwin = [2, 1]).

4.10. Electrophysiological data normalization

Two different baselines were used: (1) signal recorded during the resting state (i.e., the first 5 min of each block without visual stimulation) was used as the baseline for all trials in that block; (2) signal 2 s before each trial onset was used as the baseline for that trial. When using resting-state signal as the baseline, we excluded the signal of the first 30 s from the baseline to reduce the effect of the OFF trial from the previous session. Each type of neuronal signal (MUA power or LFP spectrogram of each frequency) was normalized (or Z-score normalized) by subtracting and then dividing the corresponding mean (or standard deviation) which was derived from the baseline to get the neuronal signal percentage change (or Z-score). The number of trials for electrophysiological data was summarized in Table 2.

4.11. Data and code availability statement

- This manuscript did not use publicly available datasets.

- Raw data associated with any figures can be provided upon request.

- There is no restrictions on data availability.

Supplementary Material

Refer to Web version on PubMed Central for supplementary material.

Acknowledgments

Data availability

Data will be made available on request.

References

Angenstein F, Kammerer E, Scheich H, 2009. The BOLD response in the rat hippocampus depends rather on local processing of signals than on the input or output activity. A combined functional MRI and electrophysiological study. J. Neurosci 29, 2428–2439. [PubMed: 19244518]

Bailey CJ, Sanganahalli BG, Herman P, Blumenfeld H, Gjedde A, Hyder F, 2013. Analysis of time and space invariance of BOLD responses in the rat visual system. Cereb. Cortex 23, 210–222. [PubMed: 22298731]

Burlingham CS, Ryoo M, Roth ZN, Mirbagheri S, Heeger DJ, Merriam EP, 2022. Task-related hemodynamic responses in human early visual cortex are modulated by task difficulty and behavioral performance. eLife 11, e73018. [PubMed: 35389340]

Burns SP, Xing D, Shapley RM, 2010. Comparisons of the dynamics of local field potential and multiunit activity signals in macaque visual cortex. J. Neurosci 30, 13739–13749. [PubMed: 20943914]

Buxton RB, Wong EC, Frank LR, 1998. Dynamics of blood flow and oxygenation changes during brain activation: the balloon model. Magn. Reson. Med 39, 855–864. [PubMed: 9621908]

Buzsaki G, Anastassiou CA, Koch C, 2012. The origin of extracellular fields and currents–EEG, ECoG, LFP and spikes. Nat. Rev. Neurosci 13, 407–420. [PubMed: 22595786]

Cardoso MMB, Lima B, Sirotin YB, Das A, 2019. Task-related hemodynamic responses are modulated by reward and task engagement. PLoS Biol. 17, e3000080. [PubMed: 31002659]

Dinh TNA, Jung WB, Shim HJ, Kim SG, 2021. Characteristics of fMRI responses to visual stimulation in anesthetized vs. awake mice. Neuroimage 226, 117542. [PubMed: 33186719]

Drew PJ, Mateo C, Turner KL, Yu X, Kleinfeld D, 2020. Ultra-slow oscillations in fMRI and resting-state connectivity: neuronal and vascular contributions and technical confounds. Neuron 107, 782–804. [PubMed: 32791040]

Drew PJ, Winder AT, Zhang Q, 2019. Twitches, blinks, and fidgets: important generators of ongoing neural activity. Neuroscientist 25, 298–313. [PubMed: 30311838]

Echagarruga CT, Gheres KW, Norwood JN, Drew PJ, 2020. nNOS-expressing interneurons control basal and behaviorally evoked arterial dilation in somatosensory cortex of mice. eLife 9, e60533. [PubMed: 33016877]

Goense JB, Logothetis NK, 2008. Neurophysiology of the BOLD fMRI signal in awake monkeys. Curr. Biol 18, 631–640. [PubMed: 18439825]

Griffis JC, Elkhetali AS, Vaden RJ, Visscher KM, 2015. Distinct effects of trial-driven and task Set-related control in primary visual cortex. Neuroimage 120, 285–297. [PubMed: 26163806]

Kajikawa Y, Schroeder CE, 2011. How local is the local field potential? Neuron 72, 847–858. [PubMed: 22153379]

Kayser C, 2004. A comparison of hemodynamic and neural responses in cat visual cortex using complex stimuli. Cereb. Cortex 14, 881–891. [PubMed: 15084493]

Kwong KK, Belliveau JW, Chesler DA, Goldberg IE, Weisskoff RM, Poncelet BP, Kennedy DN, Hoppel BE, Cohen MS, Turner R, et al. , 1992. Dynamic magnetic resonance imaging of human brain activity during primary sensory stimulation. Proc. Natl. Acad. Sci. U. S. A 89, 5675–5679. [PubMed: 1608978]

Larsson J, Solomon SG, Kohn A, 2016. fMRI adaptation revisited. Cortex 80, 154–160. [PubMed: 26703375]

Lee AM, Hoy, Jennifer L, Bonci A, Wilbrecht L, Stryker, Michael P, Niell, Cristopher M, 2014. Identification of a brainstem circuit regulating visual cortical state in parallel with locomotion. Neuron 83, 455–466. [PubMed: 25033185]

Lima B, Cardoso MM, Sirotin YB, Das A, 2014. Stimulus-related neuroimaging in task-engaged subjects is best predicted by concurrent spiking. J. Neurosci 34, 13878–13891. [PubMed: 25319685]

Logothetis NK, Pauls J, Augath M, Trinath T, Oeltermann A, 2001. Neurophysiological investigation of the basis of the fMRI signal. Nature 412, 150–157. [PubMed: 11449264]

Lu H, Clingman C, Golay X, van Zijl PCM, 2004. Determining the longitudinal relaxation time (T1) of blood at 3.0 Tesla. Magn. Reson. Med 52, 679–682. [PubMed: 15334591]

Musall S, Kaufman MT, Juavinett AL, Gluf S, Churchland AK, 2019. Single–trial neural dynamics are dominated by richly varied movements. Nat. Neurosci 22, 1677–1686. [PubMed: 31551604]

Niell CM, Stryker MP, 2010. Modulation of visual responses by behavioral state in mouse visual cortex. Neuron 65, 472–479. [PubMed: 20188652]

Nir Y, Fisch L, Mukamel R, Gelbard-Sagiv H, Arieli A, Fried I, Malach R, 2007. Coupling between neuronal firing rate, gamma LFP, and BOLD fMRI is related to interneuronal correlations. Curr. Biol 17, 1275–1285. [PubMed: 17686438]

Nunez-Elizalde AO, Krumin M, Reddy CB, Montaldo G, Urban A, Harris KD, Carandini M, 2022. Neural correlates of blood flow measured by ultrasound. Neuron 110, 1631–1640 e1634. [PubMed: 35278361]

Ogawa S, Tank DW, Menon R, Ellermann JM, Kim SG, Merkle H, Ugurbil K, 1992. Intrinsic signal changes accompanying sensory stimulation: functional brain mapping with magnetic resonance imaging. Proc. Natl. Acad. Sci. U. S. A 89, 5951–5955. [PubMed: 1631079]

Parabucki A, Lampl I, 2017. Volume conduction coupling of whisker-evoked cortical LFP in the mouse olfactory bulb. Cell Rep. 21, 919–925. [PubMed: 29069599]

Pauling L, Coryell CD, 1936. The magnetic properties and structure of hemoglobin, oxyhemoglobin and carbonmonoxyhemoglobin. Proc. Natl. Acad. Sci 22, 210–216. [PubMed: 16577697]

Ray S, Maunsell JH, 2011. Different origins of gamma rhythm and high-gamma activity in macaque visual cortex. PLoS Biol. 9, e1000610. [PubMed: 21532743]

Roth ZN, Ryoo M, Merriam EP, 2020. Task-related activity in human visual cortex. PLoS Biol. 18, e3000921. [PubMed: 33156829]

Saleem AB, Lien AD, Krumin M, Haider B, Rosón MR, Ayaz A, Reinhold K, Busse L, Carandini M, Harris KD, 2017. Subcortical source and modulation of the narrowband gamma oscillation in mouse visual cortex. Neuron 93, 315–322. [PubMed: 28103479]

Schröder S, Steinmetz NA, Krumin M, Pachitariu M, Rizzi M, Lagnado L, Harris KD, Carandini M, 2020. Arousal modulates retinal output. Neuron 107, 487–495 e489. [PubMed: 32445624]

Shmuel A, Augath M, Oeltermann A, Logothetis NK, 2006. Negative functional MRI response correlates with decreases in neuronal activity in monkey visual area V1. Nat. Neurosci 9, 569–577. [PubMed: 16547508]

Sirotin YB, Das A, 2009. Anticipatory haemodynamic signals in sensory cortex not predicted by local neuronal activity. Nature 457, 475–479. [PubMed: 19158795]

Stringer C, Pachitariu M, Steinmetz N, Reddy CB, Carandini M, Harris KD, 2019. Spontaneous behaviors drive multidimensional, brainwide activity. Science 364, eaav7893.

Turner KL, Gheres KW, Proctor EA, Drew PJ, 2020. Neurovascular coupling and bilateral connectivity during NREM and REM sleep. eLife 9, e62071. [PubMed: 33118932]

Uhlirova H, Kılıç K, Tian P, Thunemann M, Desjardins M, Saisan PA, Sakadži S, Ness TV, Mateo C, Cheng Q, 2016. Cell type specificity of neurovascular coupling in cerebral cortex. eLife 5, e14315. [PubMed: 27244241]

Van Camp N, Verhoye M, Van der Linden A, 2006. Stimulation of the rat somatosensory cortex at different frequencies and pulse widths. NMR Biomed. 19, 10–17. [PubMed: 16408324]

Viswanathan A, Freeman RD, 2007. Neurometabolic coupling in cerebral cortex reflects synaptic more than spiking activity. Nat. Neurosci 10, 1308–1312. [PubMed: 17828254]

Weber AI, Fairhall AL, 2019. The role of adaptation in neural coding. Curr. Opin. Neurobiol 58, 135–140. [PubMed: 31569061]

Winder AT, Echagarruga C, Zhang Q, Drew PJ, 2017. Weak correlations between hemodynamic signals and ongoing neural activity during the resting state. Nat. Neurosci 20, 1761–1769. [PubMed: 29184204]

Zhang Q, Cramer SR, Ma Z, Turner KL, Gheres KW, Liu Y, Drew PJ, Zhang N, 2022. Brain-wide ongoing activity is responsible for significant cross-trial BOLD variability. Cereb. Cortex
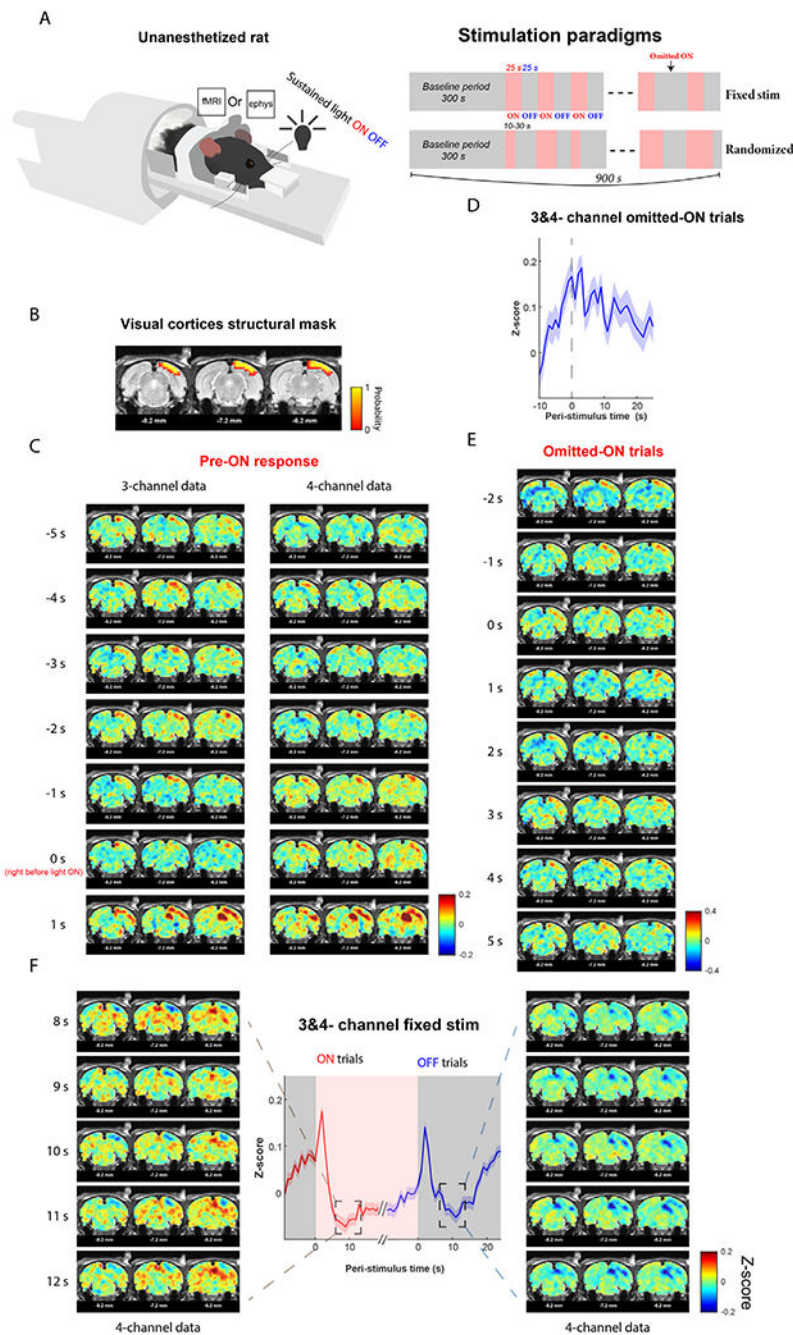
Fig. 1.
(A) Two visual stimulation paradigms were used for separate fMRI or electrophysiological recordings in unanesthetized rats. The ON/OFF duration for fixed stimulations was 25 s. The ON/OFF duration for randomized stimulations was drawn from a uniform distribution of 10 – 30 s per trial. The first 5 min of resting-state recording without visual stimulation was used as the baseline for the whole run (15 min). (B) Structural mask for the visual cortices, including V1 and V2. Color code was based on the probability of each voxel belonging to the visual cortices. (C) Averaged fMRI frames around the light onset during

fixed stimulations. A subgroup of voxels in the rVA showed positive activation before the light onset in the fMRI data, and the pattern was consistent across the datasets collected with the 3- and 4- channel coils. The light was ON right after the collection of the fMRI frames at 0 s. (D) Averaged time course of the rVA* during omitted-ON trials. (E) Averaged fMRI frames around the potential light onset during omitted-ON trials. (F) Averaged ON/OFF (red/blue) time courses of the rVA* during fixed stimulations. Averaged fMRI frames (4-channel data) during the undershoot period (8 – 12 s) for ON and OFF trials were shown on the left and right, respectively. Shaded area indicates SEM over all trials.
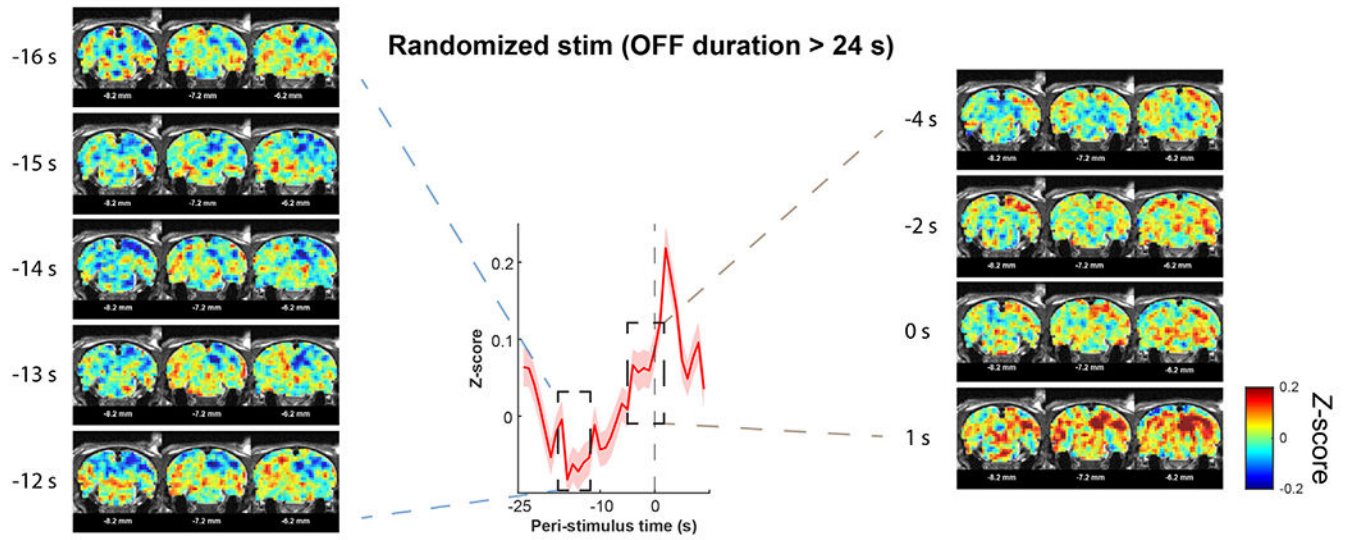
Fig. 2.

Averaged fMRI frames and time course of rVA* during randomized stimulations, with the OFF durations in the immediate preceding OFF trials longer than 24 s. Shaded area indicates SEM over all trials included.
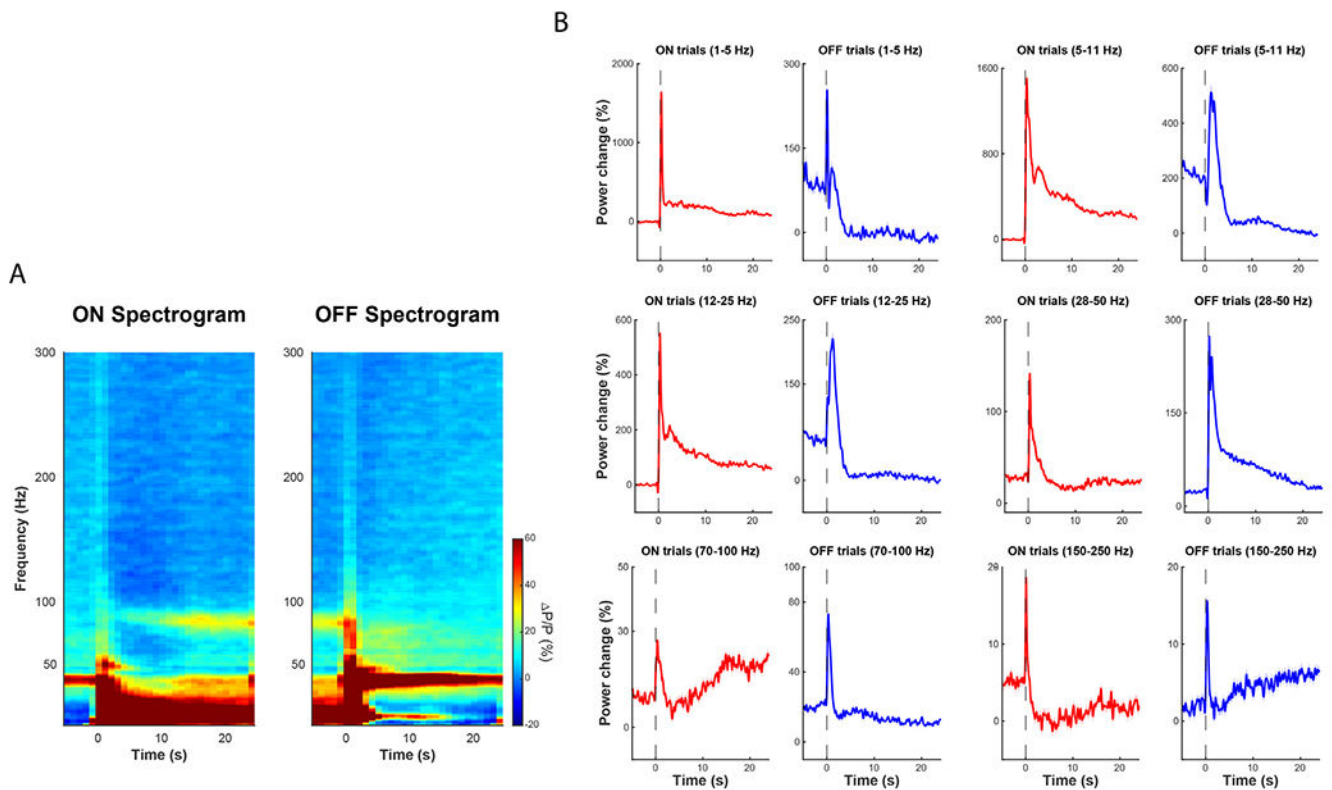
Fig. 3.

(A) Averaged ON/OFF time-frequency spectrograms during the fixed stimulations. (B) Averaged ON/OFF time courses of LFPs power in 6 frequency ranges: 1 – 5 Hz (delta range), 5 – 11 Hz (theta range), 12 – 25 Hz (alpha to beta range), 28 – 50 Hz (low gamma range), 70 – 100 Hz (gamma range), and 150 – 250 Hz. The specific band of LFP power was normalized to the resting-state (without visual stimulations) baseline by subtracting the mean and then dividing the mean of the baseline LFP power of the corresponding frequency band. Shaded area indicates SEM over all trials.
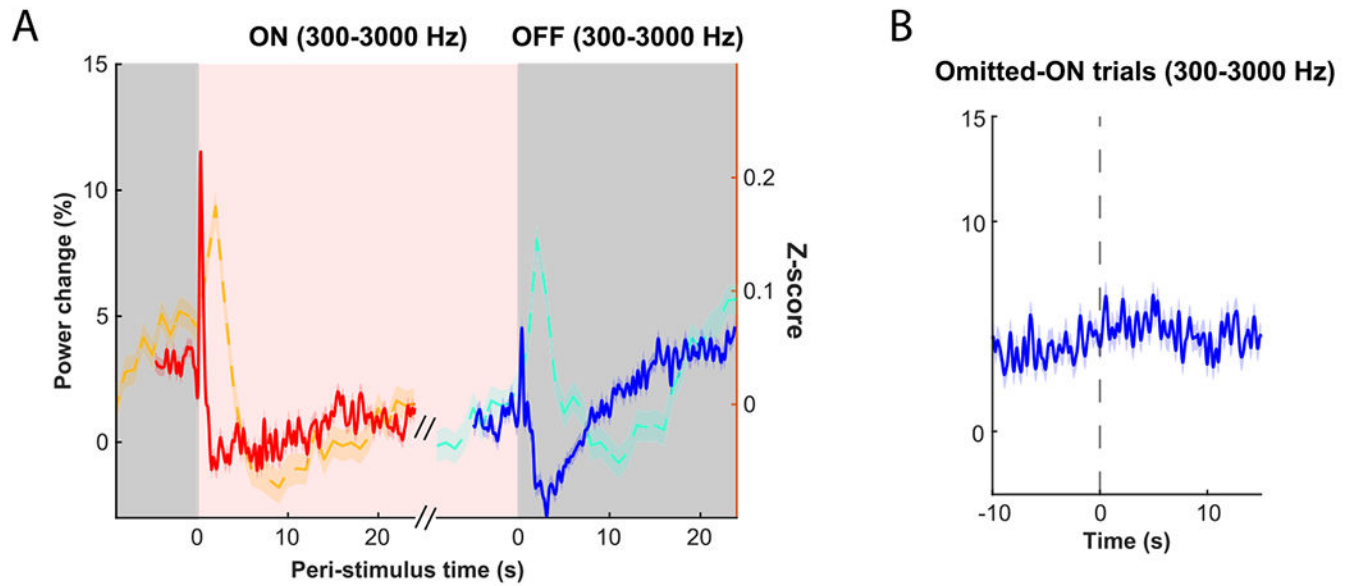
Fig. 4.

(A) Averaged ON/OFF time courses of MUA (300 – 3000 Hz) power during the fixed stimulations. Dashed lines indicate the BOLD signal from Fig. 1F. (B) Averaged time courses of MUA (300 – 3000 Hz) power during the omitted-ON trials. The MUA power was normalized to the resting-state (without visual stimulations) baseline by subtracting the mean and then dividing the mean of the baseline MUA power. Shaded area indicates SEM over all trials.

Table 1

Number of trials for fMRI data.

3-channel coil fixed stimulation		4-channel coil fixed stimulation			4-channel coil randomized stimulation	
ON tril	OFF tril	Omitted-ON trial	ON trial	OFF trial	Omitted-ON trial	ON trial (OFF duration in the preceding OFF trial > 24 s)	All ON trial (OFF duration in the preceding OFF trial 10 – 30 s)
759	759	60	918	918	118	336	1086

Table 2

Number of trials for electrophysiological data.

Fixed stimulation			Randomized stimulation	
ON trial	**OFF trial**	**Omitted-ON trial**	**ON trial (OFF duration in the preceding OFF trial > 18 s)**	**OFF trial (OFF duration in the current trial > 18 s)**
1469	1469	400	304	324